Journal of Materials Chemistry A

Accepted Manuscript

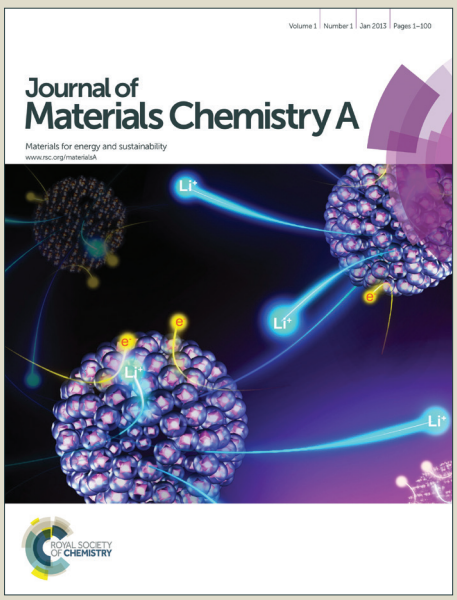

ROYAL SOCIETY OF CHEMISTRY

www.rsc.org/materialsA

Journal of Materials Chemistry A

Cite this: DOI: 10.1039/c0xx00000x

ARTICLE TYPE

www.rsc.org/xxxxxx

Hierarchically porous nitrogen-rich carbon derived from wheat straw as an ultrahigh-rate anode for lithium ion battery

Li Chen,[a] Yongzhi Zhang,[b] Chaohong Lin,[c] Wen Yang,[c] Yan Meng,[c] Yong Guo,[a] Menglong Li [*a] and Dan Xiao [*a,b]

Received (in XXX, XXX) Xth XXXXXXXXX 20XX, Accepted Xth XXXXXXXXX 20XX
DOI: 10.1039/b000000x

A facile, economical and effective method to produce hierarchically porous nitrogen-rich carbon (HPNC) derived from wheat straw has been reported. Acid pretreatment is introduced before KOH activation, and plays a role of promotion to form thinner pore walls. Without any N-doping, the N content is as high as 5.13%. The HPNC used as anode for Li-ion batteries exhibits a superior specific capacity of 1470 mAh g^{-1} at 0.037 A g^{-1}, and possesses an ultrahigh rate capability of 344 mAh g^{-1} at 18.5 A g^{-1}. Even at extremely high current density of 37 A g^{-1}, the reversible capacity is still as high as 198 mAh g^{-1}.

.

Introduction

In parallel with the aggravating energy and environmental problems such as pollution, fossil fuel depletion and global warming rise, interests in clean and renewable energy materials as well as their devices have spiked in recent years.[1] One field in particular has attracted attention: carbon materials for manufacturing anodes for the Li-ion batteries (LIBs, the energy storage device currently dominating the battery market with its wide use in portable electronic gadgets such as laptop computers, digital cameras, cell phones, and so on).[2-4] It is well known that graphite is the most commonly used anode carbon material for commercial rechargeable lithium batteries because of its low cost and low electrochemical potential with respect to lithium metal.[5,6] However, its limited storage capacity (372 mAh g^{-1}) and rate performance do not meet the requirement for high-energy and high power LIBs which are demanded ever-increasingly and urgently by the widespread application in electric or hybrid electric vehicles.[7-10]

Porous carbon materials, which offer large electrode/electrolyte interface for the charge-transfer reaction, and facilitate ion transport by providing shorter diffusion pathways, are strongly recommended for the fabrication of high-performance electrodes.[11,12] Meanwhile, as a renewable source, biomass has attracted a great deal of attention in the preparation of carbon materials,[13] because of its low value, huge amount, rapid regeneration, easy access and environmental friendship.[14] Therefore, porous carbons for LIBs anodes obtained from biomass have been explored with sources as diverse as cherry stones,[15,16] olive,[16] alginic acid,[17] mangrove charcoal,[18] rice husk[19,20] and straw,[21] peanut shells,[22] pinecone hull,[23] and banana fibers.[24] However, anodic carbon materials derived from biomass with both high capacity and high rate capability were rarely been reported.

As a by-product of wheat which is the most widespread cereal crops, wheat straw has many uses, including fuel, livestock fodder, construction materials, and papermaking et al. However, most of wheat straws (about 2 hundred millions tons annually in China alone)[25] are still burned directly in field, causing serious air pollution. Therefore, the consumption and application of wheat straw have become an important issue that needed to be solved imperiously. Wheat straw was reported that it possessed natural plant fiber structure and this structure could provide an opportunity to prepare activated carbon for supercapacitor.[26] Similarly, the by-product of rice, rice husk and rice straw that had been activated by KOH as carbon anodes, exhibited high capacities.[20,21] However, their rate performance and stability were unsatisfactory.

On the other hand, electrochemical performance of porous carbons can be further improved by modifying functional groups (such as N, B, S and P) for the presence of these elements at the carbon surface can enhance the reactivity and provide extra Li-ion storage sites.[11,27-30] Among these researches, egg white as model protein-based precursor was applied in produce mesoporous N-rich carbons as battery anodes and supercapacitors with ultra-high capacity (1780 mA h g^{-1} as LIB anode at 100 mA g^{-1} and 390.4 F g^{-1} as electrochemical capacitor electrode at 250 mA g^{-1}), which is a persuasive example that biomass was used to prepare carbon materials of energy storage.[27]

In this report, we present a simple and economic strategy for the preparation of hierarchically porous nitrogen-rich carbon (HPNC)

derived from wheat straw. Wheat straw is not only composed of cellulose, hemicellulose, lignin, and some trace metallic elements, but also crude protein which is suitable as a natural nitrogen source,[31] so it is an ideal precursor for preparation of nitrogen-rich carbons. By treatment, the HPNC with 5.13 wt% nitrogen and thin pore walls was obtained. The hierarchically porous nitrogen-rich structure can offer more sites for the storage and insertion of Li ions. The thin pore walls can accelerate electrolyte diffusion and Li-ion transport. Given all this, the obtained HPNC as anode of LIBs shows high capacity, superhigh rate and favorable stability, and this approach provides a substitute for graphite production and offers a solution for the pollution issues.

Experimental section

Preparation of HPNC

The raw material was cleaned by deionized water and dried. The prepared wheat straw was refluxed with 2 mol L^{-1} HCl solution at 120 ℃ in oil bath for 1h. After leaching, the sample was thoroughly washed with deionized water until the filtrate was free from acid. After drying, the sample was immersed in KOH solution (the weight ratio of the sample to KOH was 1:3 in the mixed system) for 24 h, then dried in the oven at 120℃. The following high temperature pyrolysis was carried out at 700℃ for 1h in a horizontal tube furnace under a high-purity Ar_2 atmosphere. The carbonaceous product was washed with deionized water to neutral. At last, HPNC was obtained after drying and crushed. The synthetic steps and production of each step are shown in Fig. S1. As a reference, the nonactivated wheat straw (NWS) and the material only activated by KOH (AWS) were prepared accordingly.

General characterization

The obtained products were subjected to various characterization techniques. The specific surface areas, total pore volume and average pore diameter were determined from N_2 adsorption/desorption isotherms at 196℃, using an automated gas sorption system (Quantachrome NOVA 1000e apparatus). Before each measurement, the sample was degassed in vacuum at 200℃ for 3 h. X-ray diffraction (XRD) measurements were performed on a TD-3500 X-ray powder diffractometer (Tongda, China). X-ray photoelectron spectra (XPS) were acquired on a Kratos XSAM 800 spectrometer (Manchester, UK). Field emission scanning electron microscopy (FESEM) images and energy dispersive spectra (EDS) were obtained with a Hitachi S4800 scanning electron microscope (Tokyo, Japan). Transmission electron microscopy (TEM) and high-resolution transmission electron microscopy (HRTEM) images were acquired on a FEI Tecnai G2 20 TEM (Hillsboro, OR, USA) operating at 200 kV. Raman spectra was detected on a Confocal LabRAM HR800 spectrometer, HORIBA Jobin Yvon, France. Elemental analysis was done by using a EuroEA3000 (Leeman, USA) Analyzer. Inductively coupled plasma atomic emission spectroscopy (ICP-AES) was detected by IRIS Advantage (ThermoElemental, USA). Digital photographs were taken by NIKON D3100 DSLR Camera and the microstructure photograph of porous fibers was obtained through the light microscope WSB-100 (Weiscope, China).

Electrochemical measurements

The electrochemical behavior of the HPNC anode material was evaluated using a coin-type cell (2032 type). To prepare working electrodes, a mixture of active material, acetylene black and poly(vinyl difluoride) (PVDF) at a weight ratio of 80 : 10 : 10 was pasted onto a Cu foil. The obtained electrodes with mass loading of around 8 mg cm^{-2} were assembled in an argon-filled glove box using lithium metal as the counter electrodes. The electrochemical characteristics were examined between 0 V and 3 V. The cyclic voltammograms (CV) was obtained at a scanning rate of 0.1 mV s^{-1}, on an Autolab PGSTAT 302 electrochemical workstation (Eco Chemie B.V., Amsterdam, the Netherlands). Electrochemical impedance spectroscopy (EIS) was carried out in the frequency range 0.01–100 kHz at a charged stage with an applied amplitude of 5 mV.

Results and Discussion

Wheat straw has been chosen as raw material to prepare HPNC not only because it is widespread, abundant, available easily and proteinaceous, but also because it possesses lots of porous fibers, as digital image shown in Fig. S2. This natural porous fibrous structures give us some enlightenment for the preparation of HPNC by KOH activation. The porous fibers possess numbers of capillaries with strong adsorbability, so that the porogen of KOH can easily access and be distributed uniformly within the wheat straw by capillarity, beneficial to obtain homogeneously porous material. And these porous fibers also afford natural channels for the diffusion of electrolyte.

The nonactivated wheat straw (NWS), the material only activated by KOH (denoted as AWS), and the sample pretreated with HCl and then activated (namely HPNC) were characterized and compared. As shown in scanning electron microscopy (SEM) image, NWS keeps the fibrous structure with smooth surface (Fig. 1a). In contrast, many pores of different diameters, which can remarkably enhance the active surface area for Li-ion storage, are found in the samples of AWS (Fig 1b) and HPNC (Fig. 1c). The transmission electron microscopy (TEM) and HR-TEM images in Fig. 1d, 1e and 1f reveal that there are some macropores, mesopores and a large amount of micropores within HPNC. Among them, the walls of macropores and large mesopores consist of amorphous texture and micropores (inset of Fig. 1e), forming an interconnected structure. The macroporous cores extend into the particles as ion-buffering reservoirs and provide a short diffusion distance to the interior surfaces when they are immersed in the electrolyte. The mesopores of the walls can provide a short ion-transport pathway, with a minimized inner-pore resistance.[32,33] Interconnected micro-, meso-, and macropores can provide low-resistant ion channels to facilitate ion transportation.[33] Meanwhile, the walls of HPNC and AWS are apparently different in thickness (insets of Fig. 1b and Fig. 1c). Actually, the thickness of the HPNC walls was measured by Imagepro-Plus software as about 60 nm, thinner than that of AWS (large than 100 nm). The thinner walls could produce a smaller inner resistance and a shorter diffusion pathway. This is because that great changes have taken place in the surface of raw material after acid treatment and pyrolysis (Fig. S3), and create many defects and cavities that facilitate the activation process.

To further examine the porous structure, the three samples were

measured by nitrogen adsorption–desorption isotherms (Fig. 2a). The specific Brunauer–Emmett–Teller (BET) surface area of AWS is 24.9 m^2 g^{-1}, whereas specific surface area of AWS and HPNC are increased significantly to 768.2 m^2 g^{-1} and 916.0 m^2 g^{-1} respectively. The pore size distribution (PSD) of AWS and HPNC were calculated using the density function theory (DFT) model and are shown in Fig. 2b. Both AWS and HPNC are mainly composed of micropores between 1.1–2.0 nm and small mesopores peaked at 2.3 nm.

X-ray diffraction (XRD) patterns of three samples are shown in Fig. 3a. Two wide characteristic peaks are located at around 25° and 43° corresponding to the (002) and (100) planes of graphite respectively, while other characteristic peaks assigned to other impurities can be observed for NWS. Moreover, no sharp peaks are observed in the XRD pattern, indicative of the amorphous state of AWS and HPNC, which is beneficial for the Li^+ intercalation and deintercalation.[34] Raman spectra presented at Fig. 3b demonstrate that HPNC exhibits the highest degree of disorder in three samples. In the Raman spectrum of carbon materials, G band (~1580 cm^{-1}) is the vibration of sp^2-bonded carbon atoms in a 2D hexagonal lattice, while the D band (~1350 cm^{-1}) is ascribed to edges, other defects, and disordered carbon.[35] The I_D/I_G intensity ratio is a measure of disorder degree and average size of the sp^2 domains.[34-36] The I_D/I_G ration of HPNC is 0.97, significantly higher than that of NWS (I_D/I_G =0.85) and AWS (I_D/I_G =0.86), represents higher degree of disorder, more edges, and more other defects (sp^3 bonded carbon, dangling bonds, vacancies, and topological defects) that favor to enhance the reversible capacities of anode and improve the Li storage ability.[34,37]

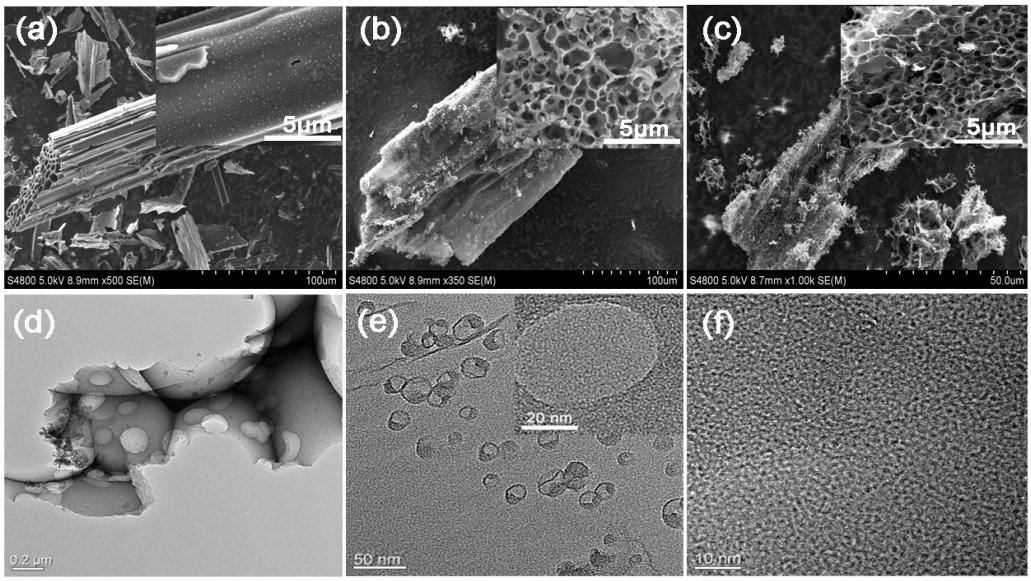

Fig. 1 SEM images of (a) NWS, (b).AWS and (c) HPNC; TEM images (d and e) and HR-TEM image (f) of HPNC. The insets of (a), (b), (c) and (e) are accordingly partial enlargements

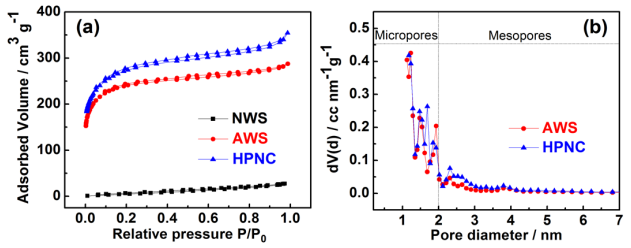

Fig. 2 (a) Nitrogen adsorption–desorption isotherms of NWS, AWS and HPNC; (b) PSD of AWS and HPNC.

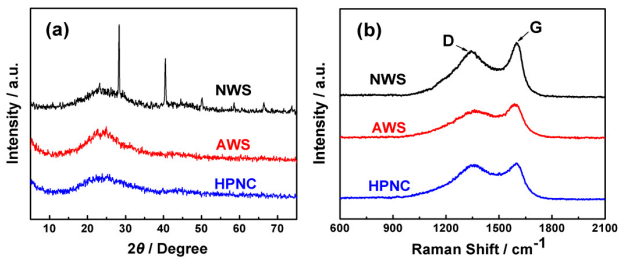

Fig. 3 (a) XRD spectra and (b) Raman spectra of NWS, AWS and HPNC.

Table 1 BET specific surface area, Raman I_D/I_G intensity ratio, Elemental analysis and content of N functionalities.

	S_{BET}/m^2 g^{-1}	Raman intensity ratio I_D/I_G	C%	N%	H%	N/C	H/C	% of total N 1s			
								N-X	N-Q	N-5	N-6
NWS	24.9	0.85	75.24	<0.5	2.86	<0.57	0.456				
AWS	768.2	0.86	69.23	1.99	3.51	2.46	0.608	8.0	16.7	33.4	41.9
HPNC	916.0	0.97	78.58	5.13	3.52	5.60	0.538	8.4	15.8	28.4	47.4

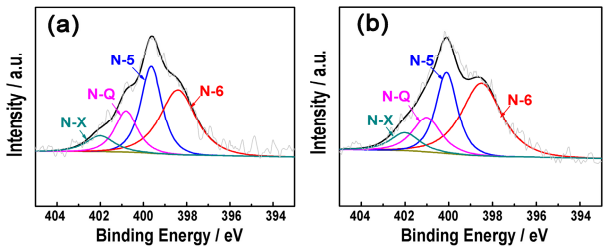

Fig. 4 N1s XPS spectra for (a) AWS and (b) HPNC.

The results of combustion element analysis are shown in Table 1. Carbonized wheat straw contains substantial hydrogen and the H/C atomic ratios of three samples are all over 0.45. High H/C atomic ratios is advantage for the reversible specific capacity since Li atoms can bind in the vicinity of H atoms in the hydrogen-containing carbons.[5] The N content of HPNC (5.13%) is much higher than other two samples (<0.5% and 1.99% respectively). Nitrogen has higher electronegativity than that of carbon for its atomic diameter is smaller. Meanwhile, there is stronger interaction between Li and nitrogen-rich carbon material because of the hybridization of nitrogen lone pair electrons with the π electrons in carbon. The electronegativity and hybridization are believed to make favorable binding sites for Li storage.[38,39] Also, the existence of N atoms devotes a large number of defects in the carbon material and produces more active sites for Li storage.[27] The X-ray photoelectron spectroscopy (XPS, Fig. 4) was applied in investigating the nature of nitrogen species at the surface. The high-resolution N 1s core level XPS spectra can be devided into 4 peaks, representing pyridinic N (N-6 at 398.5 eV ± 0.2), pyrrolic or pyridonic N (N-5 at 399.9 eV ± 0.2) quaternary N (N-Q at 400.8±0.2 eV) and oxidized N (N-X at 402.2 ±0.2 eV).[27,38,39] HPNC contains more pyridinic N, but less pyrrolic-N than AWS (Table 1). According to theoretical calculation, pyridinic N is more favorable than pyrrolic-N for Li storage.[27,39] and is a critical factor in the increase of reversible capacity.[40]

The electrochemical performance of the samples as anode material for lithium ion batteries were futher investigated. The cyclic voltammogram (CV) profiles of HPNC (Fig 5a) recorded in the first three cycles are typical for carbonaceous anode materials.[11,27] Fig. 5b, 5c, 5d show the charge/discharge profiles of NWS, AWS and HPNC at a current density of 0.037 A g^{-1}, respectively. In the first cycle, the charge/discharge profiles of HPNC present an extremely high reversible capacity (1470 mAh g^{-1}) at a current density of 0.037 A g^{-1} (Fig 5d), much higher than that of other two samples (378 mAh g^{-1} and 768 mAh g^{-1} respectively) (Fig. 5b and Fig. 5c). The initial Coulombic efficiency of HPNC is 64% at 0.037 A g^{-1} (Fig. S4), because of the large irreversible capacity during the first cycle. The initial capacity loss can be ascribed to the conversion of the carbon electrode from its pristine form to an active lithium storage host, the formation of solid electrolyte interface (SEI) that caused by the catalytic reduction of the electrolyte components on the active electrode surface and/or irreversible lithium insertion into special positions such as in the vicinity of residual H atoms in the carbon material.[12,41] As a passivation layer, the SEI layer is actually advantageous for it prevents the electrolyte from undergoing continuous decomposition on the carbon electrode. The reversible capacity of HPNC becomes stable after the first cycle, and the Coulombic efficiency of the second cycle increases dramatically to 96%. After 50th cycles, the reversible capacity of HPNC maintains at 1327 mAh g^{-1} and the Coulombic efficiency stabilized around 98% after 4 cycles, while other two samples show apparent capacity fading dropping to 459 mAh g^{-1} and 260 mAh g^{-1} respectively.

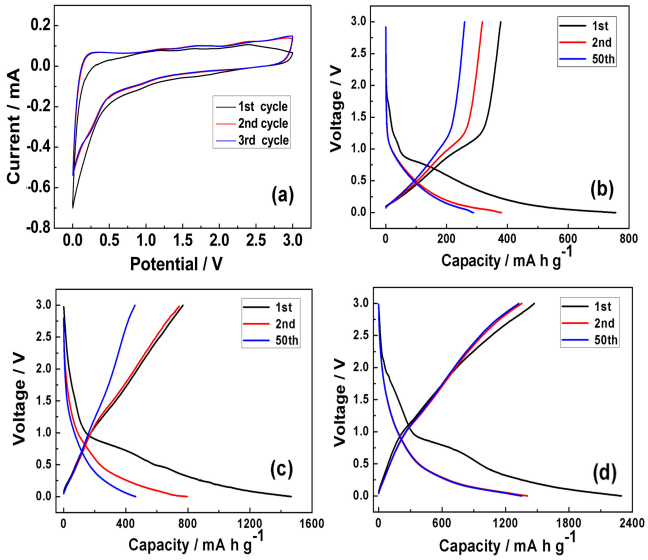

Fig. 5 (a) Cyclic voltammograms of HPNC at a scan rate of 0.1 mV s^{-1}; Charge and discharge curves of (b) NWS, (c) AWS and (d) HPNC at 0.037 A g^{-1}.

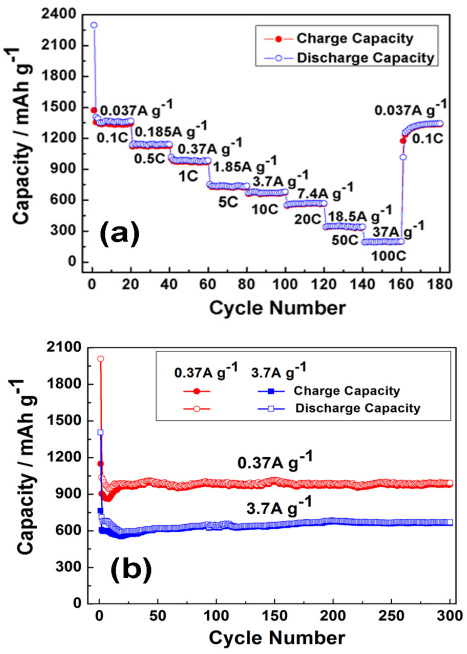

Fig. 6 (a) Capacity of HPNC over cycling at different rates; (b) Cycling performance of HPNC at 0.37 A g^{-1} and 3.7 A g^{-1}.

The reversible capacity of HPNC is not so high as that of mesoporous nitrogen-rich carbons derived from egg white[27] at low current density, partly because of its lower N content. However, its rate capability and cycling performance seem not to be affected by this shortage. Further tests show HPNC has excellent rate capability and cycling stability. Fig. 6a shows the capacity of at various current densities from 0.037 to 37 A g^{-1} each for 20 cycles. The reversible capacities are 1129 mAh g^{-1}, 975 mAh g^{-1}, 731 and 664 mAh g^{-1} at 0.185, 0.37, 1.85 and 3.7 A g^{-1} respectively. Even at extremely high current density of 7.4, 18.5 and 37 A g^{-1} (20 C, 50 C and 100 C, 1 C=372 mA g^{-1}), the reversible capacity are still as high as 566, 344 and 198 mAh g^{-1}. We compared the initial reversible capacity and rate capability of HPNC with those of some carbon materials derived from biomass as anodes for lithium ion batteries, as listed in Table S1. The rate capability of HPNC is better than those of any biomass-based carbon anodes ever reported. In addition to its considerable capacity and rate performance, HPNC also shows stable cycling performance since its reversible capacity can be recovered to 1335 mAh g^{-1} when charge–discharge current density turns back to 0.037 A g^{-1}. When tested at 0.37 A g^{-1} and 3.7 A g^{-1} respectively (Fig. 6b), the cycling performance of HPNC is as well very impressive, which as high as 976 mAh g^{-1} and 659 mAh g^{-1} respectively even after 300 cycles.

In order to understand this surface-dependent LIB performance, EIS measurements were introduced for the three samples after the performing up to 10 cycles of galvanostatic charge−discharge at 0.037 A g^{-1} and the Representative Nyquist plots are shown in Fig. 7. Each of the electrodes has two semicircles in the high-medium frequency region and an inclined line in the low frequency region respectively. The intercept at the real impedance (Z') axis in the high-frequency region should be related to internal resistance (R_s), which includes the solution resistance, the intrinsic resistance of carbon materials, and contact resistance.[42] The first semicircle corresponds to SEI resistance (R_{SEI}) and the second semicircle is attributed to charge transfer resistance (R_{ct}), while the inclined line represents lithium-diffusion process within the pores of the carbon.[43,44] It is clear that the diameters of two semicircles of HPNC are the smallest in the three electrodes, which implies that it possesses the highest electrical conductivity and the most rapid charge transfer reaction for lithium ion insertion and extraction in all the samples. The equivalent circuit has been set up in inset of Fig. 7 and some significant kinetic parameters are derived by fitting the impedance spectra to the proposed equivalent circuit using the NOVA software and listed in Table 2. The value of Constant Phase Angle Element (CPE), $Q = Y_0^{-1} (j\ \omega)^{-n}$ where Y_0 is a constant that is independent of frequency, ω is the angular frequency, $j = (-1)^{1/2}$ and n is the exponential index which represents a dispersion of relaxation. Generally, high specific area contributes to more side reactions that lower the Coulombic efficiency and thicken the SEI film. However, the R_{SEI} of HPNC is 5.09 Ω, lower than that of NWS (11.26 Ω) and AWS (5.74 Ω), meaning that Li ions in HPNC can pass through the SEI film more easily than that in NWS or AWS. It can be ascribed to the high N content of HPNC which can suppress the electrolyte decomposition and surface side reactions of electrodes with the electrolyte, reduce the formation of SEI film and enhance the Coulombic efficiency.[28] Moreover, the interconnected porous structure and thinner pore walls of HPNC are beneficial for the Li^+ intercalation and deintercalation, so the irreversible lithium trapped in the electrode will be reduced leading to a relatively high Coulombic efficiency. Therefore, HPNC exerts higher initial Coulombic efficiency (64%, while that of NWS and AWS are 50% and 52%). Meanwhile, the R_{ct} and solid-phase diffusion resistance (Q_W) of HPNC are also the lowest, account for faster charge and mass transfer in lithium insertion/extraction process and facile charge transfer at the electrode/electrolyte interface. These resluts indicate that the structures of HPNC can afford Li ions less resistance in short channels, leading to a higher rate capability.

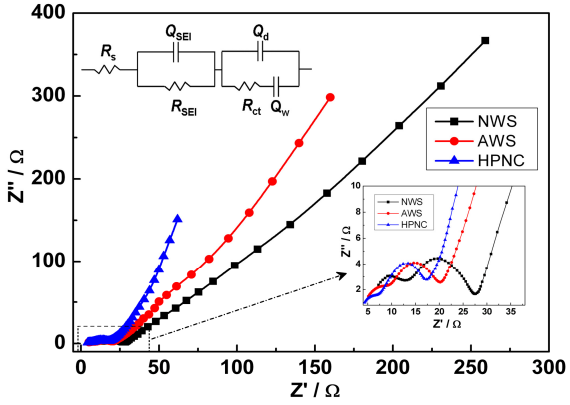

Fig. 7 Typical Nyquist plots recorded at NWS, AWS and HPNC.

Table 2. Kinetic Parameters derived from the Nyquist Plot for the samples. [a]

	R_s/Ω	R_{SEI}/Ω	Q_{SEI}		R_{ct}/Ω	Q_d		Q_w	
			Y_0/Ω^{-1}	n		Y_0/Ω^{-1}	n	Y_0/Ω^{-1}	n
NWS	4.54	11.26	7.11×10^{-6}	0.791	15.66	3.83×10^{-4}	0.754	0.022	0.605
AWS	3.82	5.74	3.94×10^{-5}	0.699	11.15	3.32×10^{-4}	0.741	0.026	0.716
HPNC	3.22	5.09	1.75×10^{-4}	0.605	8.64	2.58×10^{-4}	0.889	0.064	0.570

[a] R_s = internal resistance, R_{SEI} = SEI resistance, Q_{SEI} = SEI capacitance, R_{ct} = charge transfer resistance, Q_d = interfacial capacitance and Q_W = Warburg impedance.

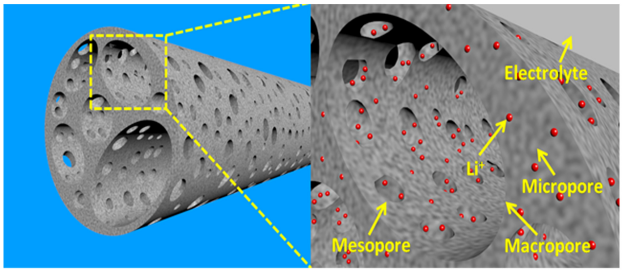

Fig. 8 Schematic representation of hierarchically porous structure and Li-ion storage in HPNC.

Acid pretreatment plays an important role in HPNC preperation. Besides small amount of crude protein, wheat straw consists of mainly three different polymers that associate with each other, namely cellulose, hemicellulose and lignin. Acid solution firstly removed the waxes that protected the fibre bundle, then disrupted the crystalline structure of cellulose and the cell-wall matrix including the connection between cellulose and lignin, and depolymerised and solubilised hemicellulose polymers.[45] Because hemicellulose accounted for the largest proportion in wheat straw,[45,46] whose solubilization could greatly increase the relative content of other components, including nitrogenous material. Meanwhile, the removal of hemicellulose increased the mean pore size of the substrate, and the disruption of crystalline structure of cellulose loosing the raw material structure,[47] maked more easily permeation of porogen. After acid treatment, the wheat straw with cellulose and lignin as carbon framework was obtained as shown in Fig. S3. And the framework could provide continuous channels for electron transportation. During KOH treatment and high-temperature pyrolysis following, KOH not only acted as a porogenic agent, but also caused swelling, leading to an increase in internal surface area, a decrease in the degree of polymerization and crystallinity, and disruption of the lignin structure.[45,46] The concept of these processes was illustrated in Fig. S5. The changes happened on components and structure of wheat straw, leading to the formation of thinner pore walls of HPNC. The ultra high rate performance can be mainly contributed to the thin pore walls, because it is more conducive to electrolyte penetration and Li-ion transfer. On the other hand, using ICP-AES test to analyse the filtrate after reflux, some trace metallic ingredients can be found, such as K, Ca, Mg, Zn, Fe et al. The elimination of metallic ingredients could produce more active sites for Li storage, thus improve the capacity of the carbon-based material. Moreover, according to EDS results (Table S2), the acid pretreatment can also remove part of Si that could induce a rapid degradation of anodes and influence the cycling stability of electrode, although it provides the highest known specific capacity for room temperature electrochemical lithiation.[48]

The reason of high specific capacity and excellent rate performance of HPNC can be concluded as follows. First of all, hierarchically porous structure offers not only large electrode/electrolyte interface for the charge-transfer reaction, but also functional pores with different dimensions which play special roles in Li-ion storage, as illustrated in Fig. 8. In the porous structure, macroporous cores serve as ion-buffering reservoirs, mesopores can accelerate the kinetic process of ion diffusion in the electrodes and improve the power density, and micropores are suggested as charge accommodation that is essential for high energy storage.[31,32,49] Furthermore, the interconnected pores provide a continuous pathway for electron transport. Secondly, metallic ingredients in wheat straw, which may occupy the bonding sites and interfere the intercalation of Li ions, are removed by acid pretreatment. This procedure not only clearly increases the relative N content, but also promotes the activated process leading to thinner walls formation that decreases the inner resistance and shortens the diffusion pathway. Last but not least, high N content without any doping can afford strong electronegativity and interaction between Li and carbon network which enhance the electronic conductivity and electrochemical stability.

Conclusions

In summary, we employed wheat straw with natural protein as carbon source to prepare hierarchically porous nitrogen-rich carbon by a facile, economic, and template-free method. With the introduction of acid pretreatment, without any N doping, the obtained HPNC with thinner pore walls and high N content exhibit high specific capacity, long-term stability, especially ultra high rate capability (the reversible capacity is as high as 198 mAh g^{-1} even at current density of 37 A g^{-1}). This approach can be easily industrialized, and become an effective solution of polluted environment. Besides application in energy storage, HPNC also can be applied in adsorbent, catalyst, water purification, gas separation and storage and other research fields.

Acknowledgements

We greatly appreciate the Natural Science Foundation of China (21275104, 21177090 and 21175094) for supporting this work.

Notes and references

[a] *College of Chemistry, Sichuan University, 29 Wangjiang Road, Chengdu 610064, PR China. Fax: +86-28-85416029; Tel: +86-28-85416029*
[b] *Institute of New Energy and Low-Carbon Technology, Sichuan University, No.24 South Section 1, Yihuan Road, Chengdu 610065, PR China. Fax:+ 86-28-6213-8325; Tel: +86-28-6213-8375*
[c] *College of Chemical Engineering, Sichuan University, No.24 South Section 1, Yihuan Road, Chengdu 610065, PR China. Fax: +86-28-85412907; Tel: +86-28-85416218*

**Corresponding author: Dan Xiao; E-mail: xiaodan@scu.edu.cn;*
**Corresponding author: Menglong Li; E-mail: liml@scu.edu.cn.*

References

1 Y. Q. Sun, Q. Wu and G. Q Shi, *Energy Environ. Sci.*, 2011, **4**, 1113.
2 M. Winter, J. O. Besenhard, M. E. Spahar, and P. Novak, *Adv. Mater.*, 1998, **10**, 725.

3 S. Flandrois and B. Simon, *Carbon*, 1999, **37**, 165.
4 M. Wissler, *J. Power Sources*, 2006, **156**, 142.
5 J. R. Dahn, T. Zheng, Y. Liu and J. S. Xue, *Science*, 1995, **270**, 590.
6 M. Winter, O. J. Besenhard, M. E. Spahr and P. Novak, *Adv. Mater.*, 1998, **10**, 725.
7 J. Thomas, *Nat. Mater.*, 2003, **2**, 705 .
8 K. Kang , Y. S. Meng, J. Bregér, C. P. Grey and G. Ceder, *Science*, 2006, **311**, 977.
9 M. Armand and J. M. Tarascon, *Nature*, 2008, ***451***, 652.
10 P. G. Bruce, B. Scrosati and J. M. Tarascon, *Angew. Chem. Int. Ed.*, 2008, **47**, 2930.
11 L. Qie, W. M. Chen, Z. H. Wang, Q. G. Shao, X. Li, L. X. Yuan, X. L. Hu, W. X. Zhang and Y. H. Huang, *Adv. Mater.*, 2012, **24**, 2047.
12 Y. S. Hu, P. Adelhelm, B. M. Smarsly, S. Hore, M. Antonietti and J. Maier, *Adv. Funct. Mater.*, 2007, **17**, 1873.
13 B. Hu, K. Wang, L. Wu, S. H. Yu, M. Antonietti and M. M. Titirici, *Adv. Mater*., 2010, **22**, 813.
14 B. Hu, S. H. Yu, K. Wang, L. Liu and X. W. Xu, *Dalton Trans.*, 2008, 5414.
15 J. C. Arrebola, A. Caballero, L. Hernán, J. Morales, M. Olivares-Marín and V. Gómez-Serrano, *J. Electrochem. Soc.*, 2010, **157**, A791.
16 A. Caballero, L. Hernán and J. Morales, *ChemSusChem*, 2011, **4**, 658.
17 X. L. Wu, L. L Chen, S. Xin, Y. X. Yin, Y.G. Guo, Q. S. Kong and Y. Z. Xia, *ChemSusChem*, 2010, **3**, 703.
18 T. Liu, R. Y. Luo, W. M. Qiao, S. H. Yoon and I. Mochida, *Electrochim. Acta*, 2010, **55**, 1696.
19 L. P. Wang, Z. Schnepp and M. M. Titirici, *J. Mater. Chem. A,* 2013, **1**, 5269.
20 G. T. Fey and C. Chen, *J. Power Sources,* 2001, **97–98**, 47.
21 F. Zhang, K. X. Wang, G. D. Li and J. S. Chen, *Electrochem. Commun.*, 2009, **11**, 130.
22 G. T. Fey, D. C. Lee, Y. Y. Lin and T. P. Kumar, Synth. Met., 2003, **139**, 71.
23 Y. J. Hwang, S. K. Jeong, K. S. Nahm, J. S. Shin and A. M. Stephan, *J. Phys. Chem. Solids*, 2007, **68**, 182.
24 A. M. Stephan, T. P. Kumar, R. Ramesh, S. Thomas, A. K. Jeong and K. S, Nahm, *Mater. Sci. Eng. A*, 2006, **430**, 132.
25 Ministry of Agriculture of the People's Republic of China, *Agr. Eng. Technol.*, 2011, **2**, 2.
26 X. L. Li, C. L. Han, X. Y. Chen and C. W. Shi, *Micropor. Mesopor. Mat.*, 2010, **131**, 303.
27 Z. Li, Z. W. Xu, X. H. Tan, H. L. Wang, C. M. B. Holt, T. Stephenson, B. C. Olsen and D. Mitlin, *Energy Environ. Sci.*, 2013, **6**, 871.
28 Z. S. Wu, W. B. Ren, L. Xu, F. Li and H. M. Cheng, *ACS Nano*, 2011, **5**, 5463.
29 H. K. Jeong, M. H. Jin, E. J. Ra, K. Y. Sheem, G. H. Han, S. Arepalli and Y. H. Lee, *ACS Nano*, 2010, **4**, 1162.
30 D. H. Jurcakova, A. M. Puziy, O. I. Poddubnaya, F. Suárez-García, J. M. D. Tascn and G. Q. Lu, *J. Am.Chem. Soc.*, 2009, **131**, 5026.
31 D. H. McCartney, H. C. Block, P. L. Dubeskj and A. J. Ohama, *Can. J. Anim. Sci.*, 2006, **86**, 443.
32 D. W. Wang, F. Li, M. Liu, G. Q. Lu, and H. M. Cheng, *Angew. Chem. Int. Ed.*, 2008, **47**, 373.
33 Y. Y. Li, Z. S. Li and P. K. Shen, *Adv. Mater.*, 2013, **25**, 2474.
34 D. Y. Pan, S. Wang, B. Zhao, M. H. Wu, H. J. Zhang, Y. Wang and Z. Jiao, *Chem. Mater.*, 2009, **21**, 3136.
35 A, Ferrari and C. J. Robertson, *Phys. Rev. B*, 2000, **61**, 14095.
36 F. Tuinstra and J. L. Koenig, *J. Chem. Phys.*, 1970, **53**, 1126.
37 L. W. Ji, Z. Lin, M. Alcoutlabi and X. W. Zhang, *Energy Environ. Sci.*, 2011, **4**, 2682.
38 Y. Mao, H. Duan, B. Xu, L. Zhang, Y. S. Hu, C. C. Zhao, Z. X. Wang, L. Q. Chen and Y. S. Yang, *Energy Environ. Sci.*, 2012, **5**, 7950.
39 C. C. Ma, X. H. Shao and D. P. Cao, *J. Mater. Chem.*, 2012, **22**, 8911.
40 Y. P. Wu, S. B. Fang and Y. Y. Jiang, *Solid State Ionics*, 1999, **120**, 117.
41 G. Ji, Y. Ma and J. Y. Lee, *J. Mater. Chem.*, 2011, **21**, 9819.
42 C. H. Huang, Q. Zhang, T. C. Chou, C. M. Chen, D. S. Su and R. A. Doong, *ChemSusChem*. 2012, **5**, 563.
43 S. Yang, X. Feng, L. Zhi, Q. Cao, J. Maier and K. Mullen, *Adv. Mater.*, 2010, **22**, 838.
44 M. S. Kim, D. Bhattacharjya, B. Z. Fang, D. S. Yang, T. S. Bae and J. S. Yu, *Langmuir*, 2013, **29**, 6754.
45 P. Kumar, D. M. Barrett, M. J. Delwiche and P. Stroeve, *Ind. Eng. Chem. Res.*, 2009, **48**, 3713.
46 Y. Sun and J. Cheng, *Bioresource Technol.*, 2002, **83**, 1.
47 A. T. W. M. Hendriks and G. Zeeman, *Bioresource Technol.*, 2009, **100**, 10.
48 M. R. Zamfir, H. T. Nguyen, E. Moyen, Y. H. Lee and D. Pribat, *J. Mater. Chem. A*, 2013, **1**, 9566..
49 H. Jiang, Pooi See Lee and C. Z. Li, *Energy Environ. Sci.*, 2013, **6**, 41.